LAWRENCE
LIVERMORE
NATIONAL
LABORATORY

LLNL-TR-400220

Atmospheric Climate Model Experiments Performed at Multiple Horizontal Resolutions

T. Phillips, G. Bala, P. Gleckler, D. Lobell, A. Mirin, R. Maxwell, D. Rotman

January 3, 2008

Disclaimer

This document was prepared as an account of work sponsored by an agency of the United States government. Neither the United States government nor Lawrence Livermore National Security, LLC, nor any of their employees makes any warranty, expressed or implied, or assumes any legal liability or responsibility for the accuracy, completeness, or usefulness of any information, apparatus, product, or process disclosed, or represents that its use would not infringe privately owned rights. Reference herein to any specific commercial product, process, or service by trade name, trademark, manufacturer, or otherwise does not necessarily constitute or imply its endorsement, recommendation, or favoring by the United States government or Lawrence Livermore National Security, LLC. The views and opinions of authors expressed herein do not necessarily state or reflect those of the United States government or Lawrence Livermore National Security, LLC, and shall not be used for advertising or product endorsement purposes.

This work performed under the auspices of the U.S. Department of Energy by Lawrence Livermore National Laboratory under Contract DE-AC52-07NA27344.

UCRL-XXXXXX

Atmospheric Climate Model Experiments Performed at Multiple Horizontal Resolutions

Thomas Phillips, Govindasamy Bala, Peter Gleckler, David Lobell,
Arthur Mirin, Reed Maxwell, and Douglas Rotman

Chemistry, Materials, Earth and Life Sciences (CMELS) Directorate
Lawrence Livermore National Laboratory (LLNL)

December 21, 2007

Laboratory Directed Research and Development (LDRD) Project 06-ERD-066

Abstract

This report documents salient features of version 3.3 of the Community Atmosphere Model (CAM3.3) and of three climate simulations in which the resolution of its latitude-longitude grid was systematically increased. For all these simulations of global atmospheric climate during the period 1980-1999, observed monthly ocean surface temperatures and sea ice extents were prescribed according to standard Atmospheric Model Intercomparison Project (AMIP) values. These CAM3.3 resolution experiments served as control runs for subsequent simulations of the climatic effects of agricultural irrigation, the focus of a Laboratory Directed Research and Development (LDRD) project.

The CAM3.3 model was able to replicate basic features of the historical climate, although biases in a number of atmospheric variables were evident. Increasing horizontal resolution also generally failed to ameliorate the large-scale errors in most of the climate variables that could be compared with observations. A notable exception was the simulation of precipitation, which incrementally improved with increasing resolution, especially in regions where orography plays a central role in determining the local hydroclimate.

1. Introduction

In principle, the global climate comprises all statistical moments of the world's weather, where "weather" signifies diverse phenomena in the atmosphere, oceans, ice sheets, land, and biota whose life cycles are short compared to the statistical averaging period. Endeavors to numerically simulate the global climate are therefore worthwhile, both to identify the primary determinants of this complex coupled system and to estimate the direction and magnitude of its potential future change.

Simulation of atmosphere-land climate entails modeling the spatio-temporal evolution of state variables of the atmospheric fluid (e.g. temperature, pressure, density, horizontally directed winds, vertical motion, etc.) and of the vegetated land surface (e.g. temperature and moisture of the canopy and soil, runoff, etc.) subject to mass, momentum, and energy forcings. Relevant energy forcings comprise, for example, the heating originating from absorption of short-wave (visible) or long-wave (infrared) radiation and from phase conversions of moisture and related physical processes such as cloud formation, convection, and turbulent heat transfer.

Because such forcings are mutually interactive (e.g. radiation with clouds, turbulent fluxes with convective processes, etc.), their governing relationships are expressed as coupled nonlinear partial differential equations. This complex mathematical system can only be solved approximately--spatially on a grid of finite resolution, and temporally by repeatedly stepping ahead in small time increments. Global climate simulations thus typically require very fast computers for their practical implementation.

Due to our incomplete understanding of the interactions of the climatic system components as well as practical computational limitations, only a partial simulation of this complex coupled system is now feasible. Moreover, many climatic investigations deliberately limit their scope to partial numerical solutions when this is thought to suffice for the problem at hand.

This is the case in our current Laboratory Directed Research and Development (LDRD) project: We are investigating the climatic effects of agricultural irrigation by employing version 3.3 of the Community Atmosphere Model (CAM3.3) that predicts variations in land-atmosphere interactions, while treating ocean and sea ice states as prescribed boundary conditions. The CAM3.3, which exemplifies the sixth generation of U.S. community climate models, was developed in a collaborative effort of the U.S. climate science community under the aegis of the National Center for Atmospheric Research (NCAR).

In climate modeling it is also common practice to differentiate numerical "control" and "sensitivity" experiments. A control experiment is a simulation of an unperturbed climate state, while a sensitivity experiment is designed to investigate the possible effect(s) of a single change in the climate system.

Our control experiments are CAM3.3 simulations of 20-year climatic history, implemented at several different latitude-longitude grid resolutions. Our sensitivity experiments also are conducted with the CAM3.3 at different horizontal resolutions, but their distinguishing feature is the inclusion of modified surface forcings to simulate the effects of agricultural irrigation. Thus, differences between an irrigation sensitivity experiment and a control experiment at the same resolution allow the potential climatic effects of irrigation to be identified. *Note, however, this document describes only the details of our control experiments at different horizontal resolutions, leaving a full discussion of the irrigation sensitivity experiments for a future journal paper.*

The remainder of this report is organized as follows. In Section 2, we summarize the principal features of the CAM3.3. Then, in a brief model validation exercise described in Section 3, we compare selected CAM3.3 climate variables simulated at different horizontal resolutions with corresponding observations, both globally and in selected regions where irrigation is commonly practiced. We close in Section 4 by summarizing the main results of these resolution changes on the control experiments. Additional details of the features of the CAM3.3 model and of our control experiments are documented in the Appendix.

2. Basic Features of the CAM3.3 Atmospheric Climate Model

Here we provide only a cursory summary of selected features of the CAM3.3 model, emphasizing technical innovations introduced subsequent to the earlier-generation CAM2 model. Key references to consult for further technical details are the NCAR report on the CAM3 model line (Collins et al. 2004), and related journal papers (Collins et al. 2006a,b).

As is generally the case in atmospheric models, state variables simulated on a specified horizontal grid are influenced by sub-grid processes that must be "parameterized" in terms of the grid-scale variables. Table 1 includes capsule descriptions of basic grid-scale and parameterized features of the CAM3.3.

A finite volume (FV) representation of atmospheric variables is adopted in our CAM3.3 experiments. In the FV framework, the evolution of variables is predicted in Lagrangian control volumes that expand or contract vertically. The horizontal dimensions of the control volumes are specified by a fixed latitude-longitude grid: our control experiments include 20-year runs at 3 different horizontal resolutions having latitude-longitude mesh sizes of 1.89x2.50 degrees, 0.94x1.25 degrees, and 0.47x0.63 degrees--designated as resolution configurations *bb*, *cc*, and *dd* respectively.

The atmospheric equations are solved at 26 vertical levels spanning the surface to 3 millibars (mb) pressure. Time stepping proceeds sequentially for the model dynamics and physics; that is, at each time step the physical processes are updated from a state that is first determined by the model dynamics, rather than updating both dynamics and physics from the same state.

Radiatively active atmospheric chemical constituents include concentrations of carbon dioxide, methane, nitrous oxide, ozone, oxygen, and chloro-fluorocarbon compounds CFC11 and CFC12 that are prescribed according to current estimates. Present-day climatologies of natural and anthropogenic aerosols (e.g. sea salt, soil-dust, volcanic, sulfate, and carbonaceous) also are specified from a chemical transport model forced with meteorological analysis. In addition, a time history of the mass of stratospheric sulfuric acid for volcanic eruptions in the recent past is included.

Table 1: Selected features of the CAM3.3 atmospheric climate model

Model Feature	Summary Description
Atmospheric representation	Finite volume (FV)
Vertical domain, levels	Surface to atmospheric pressure 3 millibars (mb) on 26 vertical levels
Horizontal domain; resolutions	Global domain; 1.89x2.50, 0.94x1.25,and 0.47x0.63 degrees latitude-longitude
Time stepping	Sequential solution of model dynamics and physics
Radiatively active chemistry	Prescribed concentrations of carbon dioxide, methane, nitrous oxide, ozone, CFC11, CFC12, oxygen, aerosols (sulfate, sea salt, carbonaceous, soil-dust, and volcanic)
Short-wave radiation	δ-Eddington approximation for scattering and absorption by molecules, cloud particles, and aerosols
Long-wave radiation	Absorption-emission scheme accounting for effects of band-overlap and the water vapor continuum
Cloud/precipitation formation	Prognostic cloud water distinguishing liquid and ice-phase condensate; diagnostic cloud fractional area
Penetrative convection	Plume ensemble updrafts computed in grid boxes where lower atmosphere is thermodynamically unstable
Boundary layer processes	Surface turbulent fluxes of heat, moisture, and momentum computed by stability-dependent formulae
Ocean boundary conditions	AMIP specifications of observed 1980-1999 monthly sea surface temperatures and sea ice extents
Land processes	Represented as in the Community Land Model version 3 (CLM3): vegetation canopy; infiltration, runoff, and drainage of moisture; diffusion of soil heat and moisture

The radiative transfer equations in the CAM3 line are more accurately approximated than in the CAM2 predecessor model. For short-wave radiation, a δ-Eddington scheme approximates scattering and absorption by chemical constituents, cloud particles, and aerosols in terms of a single upward-directed or downward-directed flux. Long-wave radiative fluxes are computed by an emission-absorption scheme that accounts for band-overlap effects of chemical constituents and water vapor, but with new terms added to approximate line-by-line calculations for the latter. Near-infrared absorption also is updated to better account for the effects of the water-vapor continuum. A mechanism for treating both short-wave and long-wave effects of volcanic aerosols is now also included.

The CAM3 line differs substantially from its model predecessors in its parameterization of cloud and precipitation formation: cloud water, ice, and precipitate are prognostically determined (i.e. these moist processes now are explicitly predicted), rather than being estimated diagnostically from other state variables, as in the predecessor CAM2 model line. This prognostic scheme includes two aspects: 1) a macro-scale component that describes the exchange of moisture between the condensate and the vapor phase, as well as the associated temperature change resulting from this phase change; and 2) a bulk microphysical component that controls the conversion from condensate to precipitate.

Cloud fractional areas in each grid box are still diagnostically determined (as in CAM2) from local thermodynamic stability, relative humidity, and convective mass flux. However, a new general treatment of the effects of geometrical cloud overlap for the radiation calculations is implemented in the CAM3 model line: the short-wave and long-wave fluxes and heating rates are computed for random cloud overlap, maximum overlap, or an arbitrary combination thereof. Adjacent cloud layers are maximally overlapped and groups of clouds separated by cloud-free layers are randomly overlapped.

As in CAM2, the representation of deep convection follows a plume approach, where an ensemble of convective scale updrafts and associated saturated downdrafts may exist whenever the atmosphere is conditionally unstable in the lower troposphere. The updraft ensemble includes plumes that are sufficiently buoyant to penetrate the unstable layer, where all plumes are assumed to have the same upward mass flux at the bottom of the convective layer. Deep convection occurs only when there is convective available potential energy (CAPE), and parcel ascent from the sub-cloud layer acts to destroy CAPE at an exponential rate using a specified adjustment time scale that is based on the effects of both updrafts and downdrafts. A companion scheme also computes the effects of shallow convection on the vertical profiles of atmospheric temperature and moisture. In addition, enhancement of atmospheric moisture by evaporation of convective precipitation has been added to the CAM3 model line.

As in previous-generation community climate models, boundary layer fluxes of heat, moisture, and momentum from the surface to the lower atmosphere and related vertical diffusivities are computed, "locally" (i.e. proportional to vertical gradients of moisture, temperatures, and winds) for thermodynamically stable or neutral conditions, and "non-locally" (counter-gradient) for thermodynamically unstable conditions, where the nonlocal calculations depend on the derived height of the boundary layer top. Moreover, because the CAM3 model line includes a specification of the fractional area of land, ocean, and ice in each grid box, flux differences due to sub-grid variations of surface types can be represented.

For our control experiments, ocean boundary conditions include observed monthly sea surface temperatures and sea ice extents for the period 1980-1999 which are prescribed according to values supplied by the Atmospheric Model Intercomparison Project (AMIP), a standard model validation exercise endorsed by the World Climate Research Programme and coordinated by LLNL's Program for Climate Model Diagnosis and

Interccomparison (Gates 1992, Gates et al. 1999). These boundary conditions were mapped appropriately for each choice *bb*, *cc*, or *dd* of horizontal resolution.

In CAM3.3, land thermodynamics and hydrology are formulated according to version 3 of the Community Land Model (CLM3) documented by Oleson et al. (2004). For each land grid cell, bare-soil and vegetated fractions are specified, where the latter may include up to 4 of a total of 16 plant functional types (PFTs) which comprise a variety of trees, grasses, shrubs, and agricultural crops. The vegetation canopy intercepts a fraction of surface precipitation, which subsequently evaporates at the potential rate. In addition, transpiration of subsurface moisture occurs via vegetation roots and stomates, where the stomatal resistance to moisture flux (and proportionate increase in sensible heat flux) varies according to vegetation type, photosynthesis rate, and carbon dioxide concentration. Calculation of surface radiative fluxes also accounts for the density and albedo of the vegetation canopy. Vertical diffusion of subsurface heat and moisture depend on local soil properties and are computed in 10 layers; infiltration and runoff of surface moisture also depend on local water table depth and orography. A river routing scheme then directs surface runoff and subsurface drainage to the model oceans.

3. CAM3.3 Control Simulations: Comparisons with Observations

In this section, we evaluate annual-mean or seasonal-mean control climates simulated by the CAM3.3 model in resolution configurations *bb*, *cc*, and *dd* relative to corresponding observational data over the period 1980-1999. This model evaluation is preliminary, in that only a few climate variables are considered, but it is carried out at both the global scale and in selected regions where irrigation is extensively practiced. A question of particular interest is whether increasing horizontal resolution produces improved simulations of the historical climate.

3.1 Vertical profiles of selected zonally averaged atmospheric climate variables

We first compare a few key atmospheric climate variables, depicted in their annual-mean vertical profiles that are averaged ("zonally") over all longitudes. For example, the vertical profile of zonally averaged, annual-mean atmospheric temperature is displayed in the top panel of Figure 1 for the CAM3.3 in resolution configuration *bb*. The corresponding observations (middle panel), as well as for the model-observational differences (bottom panel) also are shown.

Errors typical of present-day climate model simulations are apparent; in particular, upper-tropospheric temperatures (at pressures between ~300 to 150 mb) in high latitudes of both hemispheres are much too cold (by as much as -10 deg K). Model temperatures in the tropical troposphere and stratosphere are instead somewhat too warm.

Figure 1: Zonally averaged vertical profiles of annual-mean atmospheric temperature (in deg K) as a function of latitude for the 1980-1999 annual-mean climate of the CAM3.3 model in configuration *bb* (horizontal resolution 1.89x2.50 degrees latitude-longitude, left top) is compared with corresponding observational reanalysis data from the European Center for Medium Range Weather Forecasts (ECMWF, right top). Model-observational differences are shown in the bottom panel.

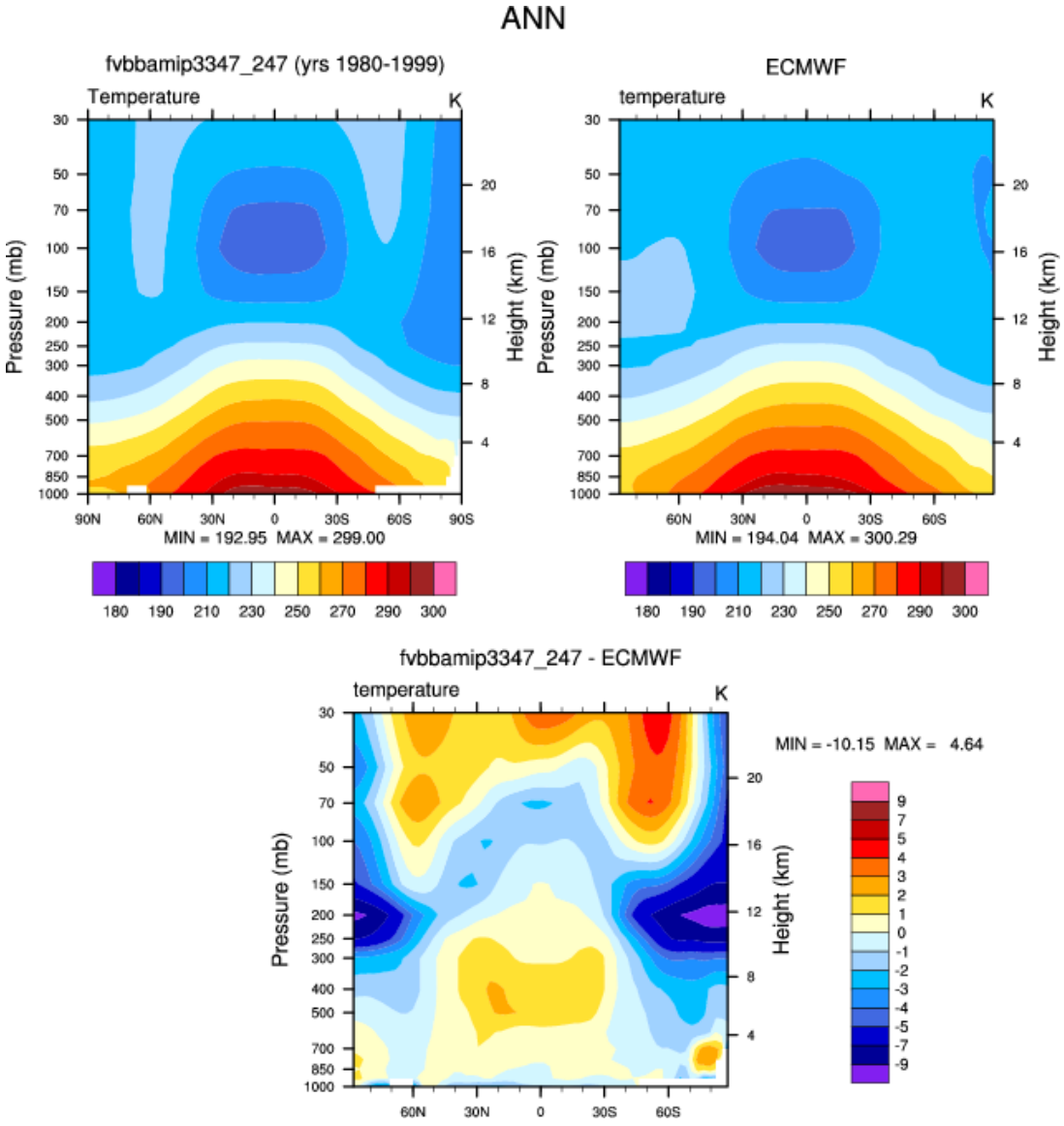

With increasing horizontal resolution corresponding to configurations *cc* and *dd* in Figure 2, the model's warm biases decrease somewhat, but the upper-tropospheric cold biases intensify by as much as ~ -1.5 deg K.

Figure 2: CAM3.3 annual-mean temperature differences from ECMWF observational data for model configurations *cc* (horizontal resolution 0.94x1.25 degrees latitude-longitude, top panel) and *dd* (horizontal resolution 0.47x0.63 degrees latitude-longitude, bottom panel).

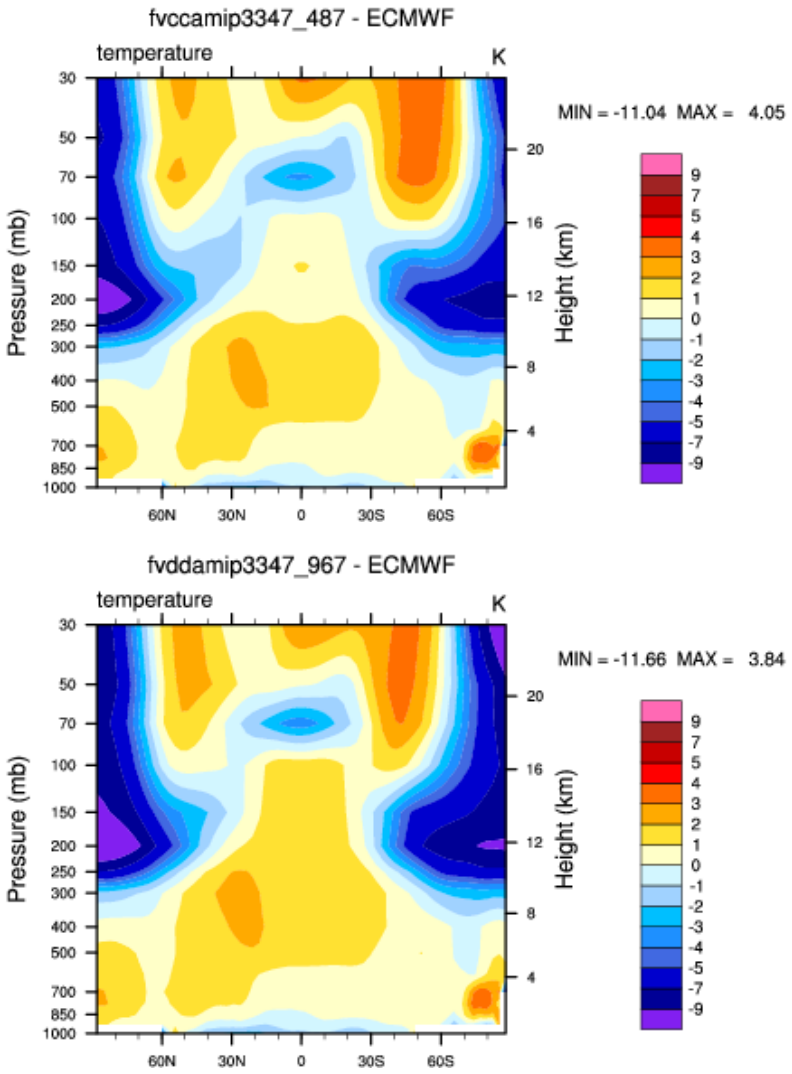

At its coarsest resolution configuration *bb*, the CAM3.3's annual-mean vertical profile of zonally averaged atmospheric specific humidity (expressed in grams of water vapor per kilogram of moist air) is qualitatively similar to observations, but differs somewhat in magnitude (Figure 3). The model's humidity biases are mostly positive, especially near the surface, but the tropical atmosphere is too dry by as much as 1 g kg^{-1} between ~900 to 600 mb.

Figure 3: As in Figure 1, except for atmospheric specific humidity (units of g water vapor per kg of moist air)

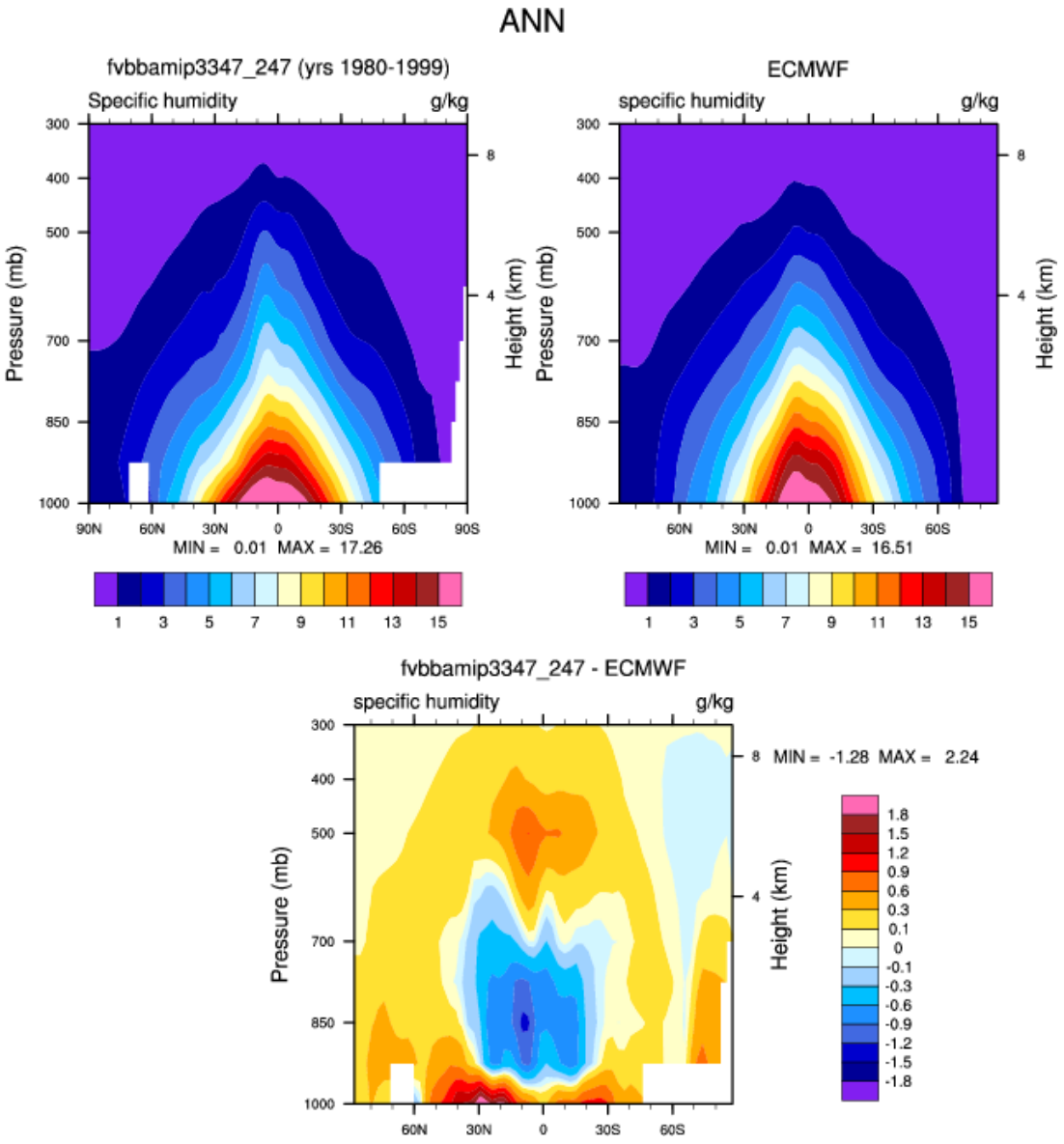

This humidity-bias pattern suggests that the model's surface evaporation is generally too strong, and that its convection scheme may entrain too much moisture in the lower tropical troposphere, and detrain too much at higher levels. The tropical negative-humidity biases also are somewhat larger at finer resolution configurations *cc* and *dd* (Figure 4).

Figure 4: As in Figure 2, except for model-observational atmospheric specific humidity differences.

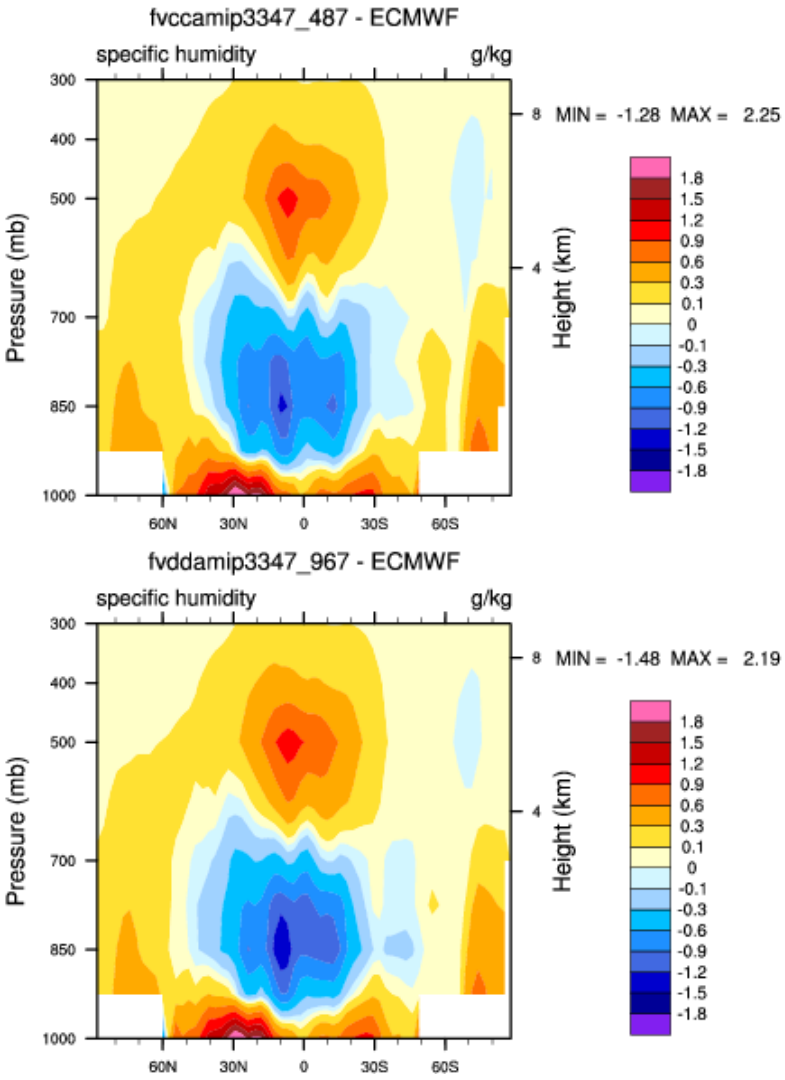

The vertical profile of a climate model's zonal (eastward- or westward-directed) winds is a telling indicator of its ability to realistically simulate atmospheric dynamics. The CAM3.3's annual-mean zonal winds simulated in resolution configuration *bb* are compared with those obtained from the ECMWF reanalysis in Figure 5.

Figure 5: As in Figure 1, except for atmospheric zonal (eastward- or westward-directed) winds (expressed in meters per second, with eastward-directed winds assigned positive values).

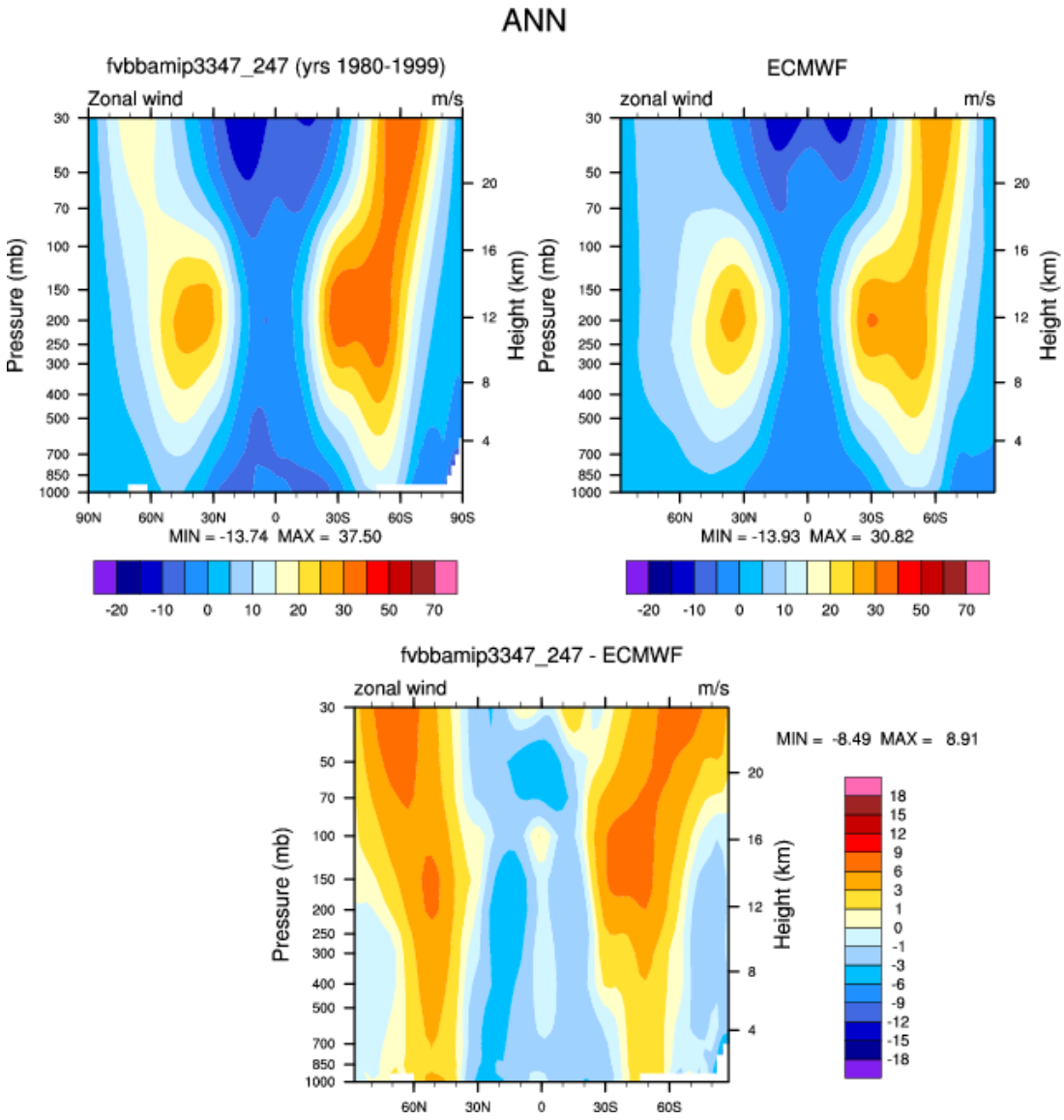

Similar to the observations, the model produces westerly (eastward-directed) extratropical winds in both hemispheres, with the greatest intensities occurring in jet stream core regions at ~ 200 mb and higher elevations. The CAM3.3 also reproduces the observed greater vertical extent of the westerlies in the Southern Hemisphere. In addition, the model correctly simulates easterly (westward-directed) winds in tropical and

polar latitudes. Despite these qualitative similarities, the model's extratropical westerlies are too intense by as much as ~9 m s^{-1}, and the magnitude of the bias in the tropical easterly zonal winds is almost as large (Figure 5, bottom panel).

For increasing horizontal resolution, the positive biases in the westerly winds markedly intensify (Figure 6), with model-observational differences as large as 15 m s^{-1} at the finest resolution *dd* (Figure 6, bottom panel).

Figure 6: As in Figure 2, except for model-observational zonal wind differences.

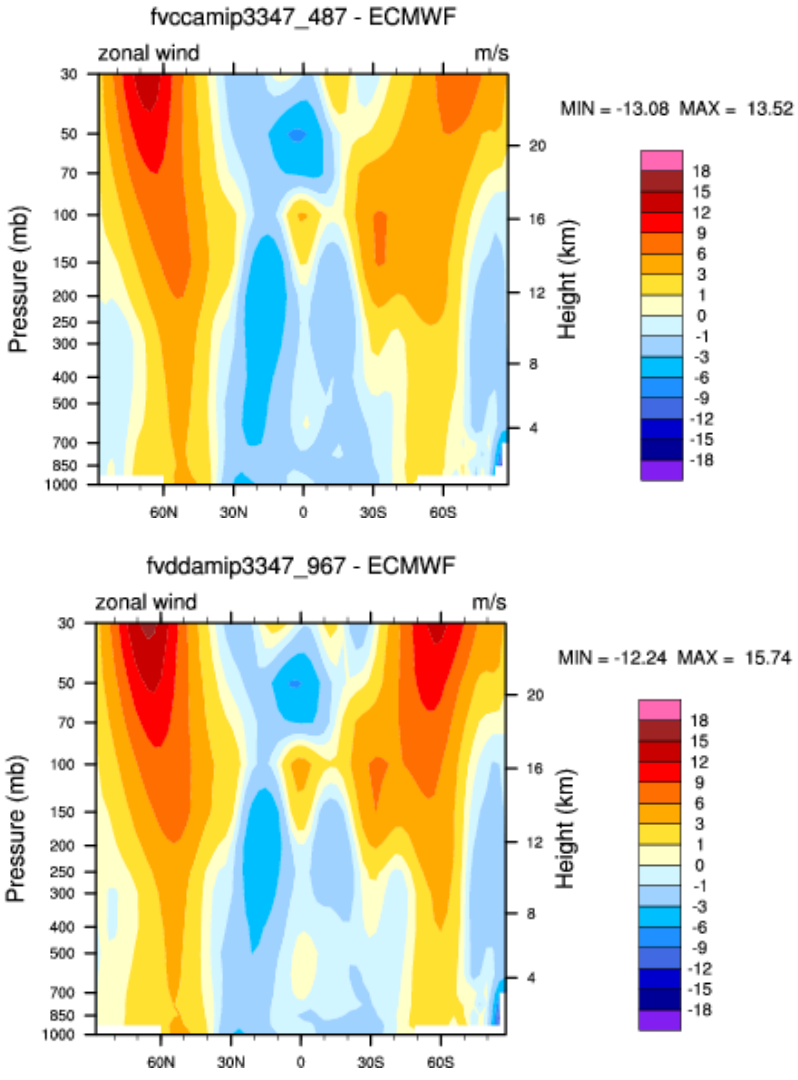

3.2 Maps of selected atmospheric climate variables in Northern Hemisphere summer

Another common depiction of a climate variable is a contoured two-dimensional mapping of its spatial variation in latitude and longitude. Figure 7 shows a contour plot of total (vertically integrated) cloud cover at resolution configuration *bb* in the model versus observations, and of their differences. These cloud-cover fields are averaged over the Northern Hemisphere summer season (i.e. June-July-August (JJA)-average values for the period 1980-1999) when the climatic effects of irrigation are likely to be most substantial.

Figure 7: Contour plots of the JJA-average total (vertically integrated) cloud cover (expressed as a percentage area), as simulated by the CAM3.3 model in the *bb* configuration (horizontal resolution 1.89x2.50 degrees latitude-longitude, top panel), and as observed from the International Satellite Cloud Climatology Project (ISCCCP, middle panel). Model-observational differences, as well as the associated global-mean bias and root-mean-square error (**rmse**), are shown in the bottom panel.

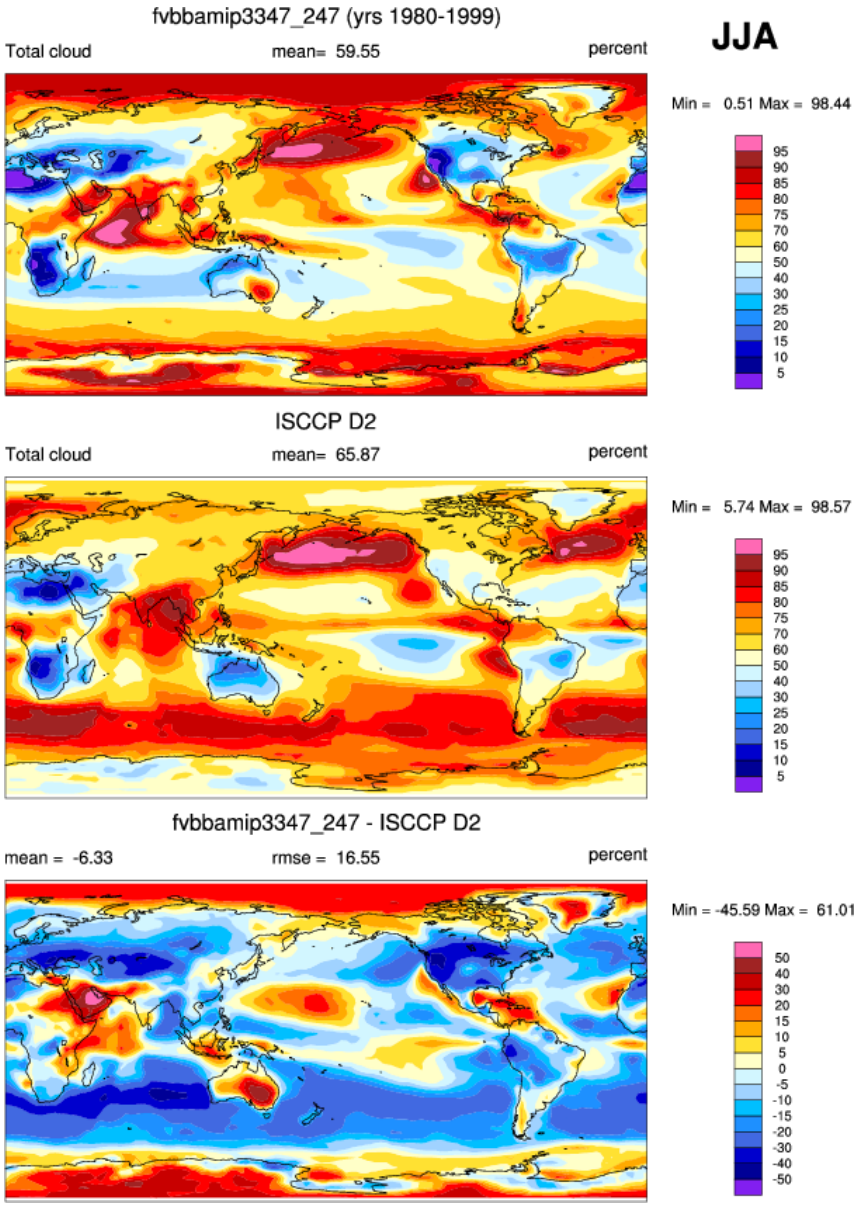

Except near the poles and in some tropical locations, the CAM3.3 in resolution configuration *bb* simulates too little total cloud cover relative to available ISCCP satellite observations (global-average bias about - 6 %). The model's global root-mean-square error (**rmse**) also is substantial (17 %) in this instance.

The model-observational difference pattern remains qualitatively similar for increasing horizontal resolution (Figure 8), but the magnitude of the overall error grows (global **rmse** values of 18 % and 20 % in configurations *cc* and *dd*, respectively).

Figure 8: JJA-average model-observational differences in total cloud cover for model configurations *cc* (0.94x1.25 degrees latitude-longitude, top panel) and *dd* (0.47x0.63 degrees latitude-longitude, bottom panel). The corresponding global-mean bias and **rmse** also are shown for each configuration.

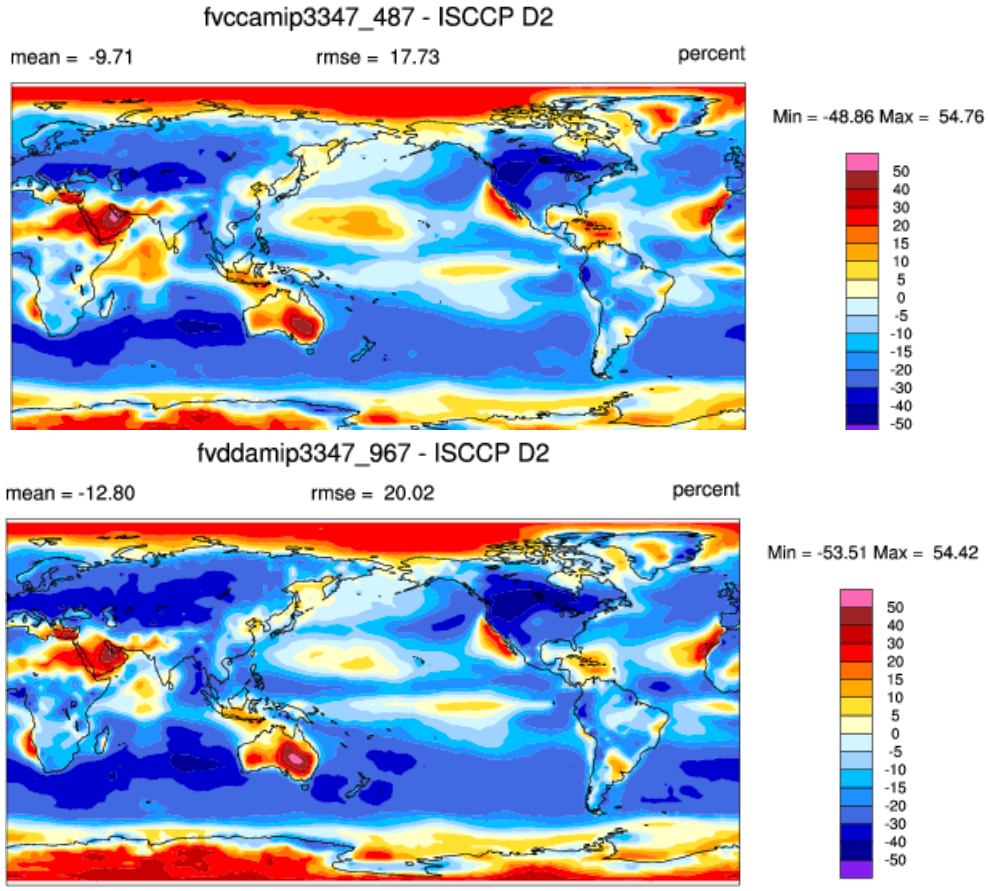

Because cloud-cover biases tend to impact the net surface energy balance, there is much consistency between the error pattern for the JJA-average cloud cover and that of the simulated continental surface air temperature in resolution configuration *bb*: where model cloud cover is too scant (Figure 7, bottom panel), continental surface air temperatures are generally too high (Figure 9, bottom panel), and vice versa.

Figure 9: As in Figure 7, except for the JJA-average CAM3.3 continental surface air temperature in resolution configuration *bb* (expressed in degr K, top panel) compared with corresponding temperature observations from the Climatic Research Unit (CRU) dataset (middle panel). Model-observational differences, as well as the associated global-average bias and **rmse**, are shown in the bottom panel.

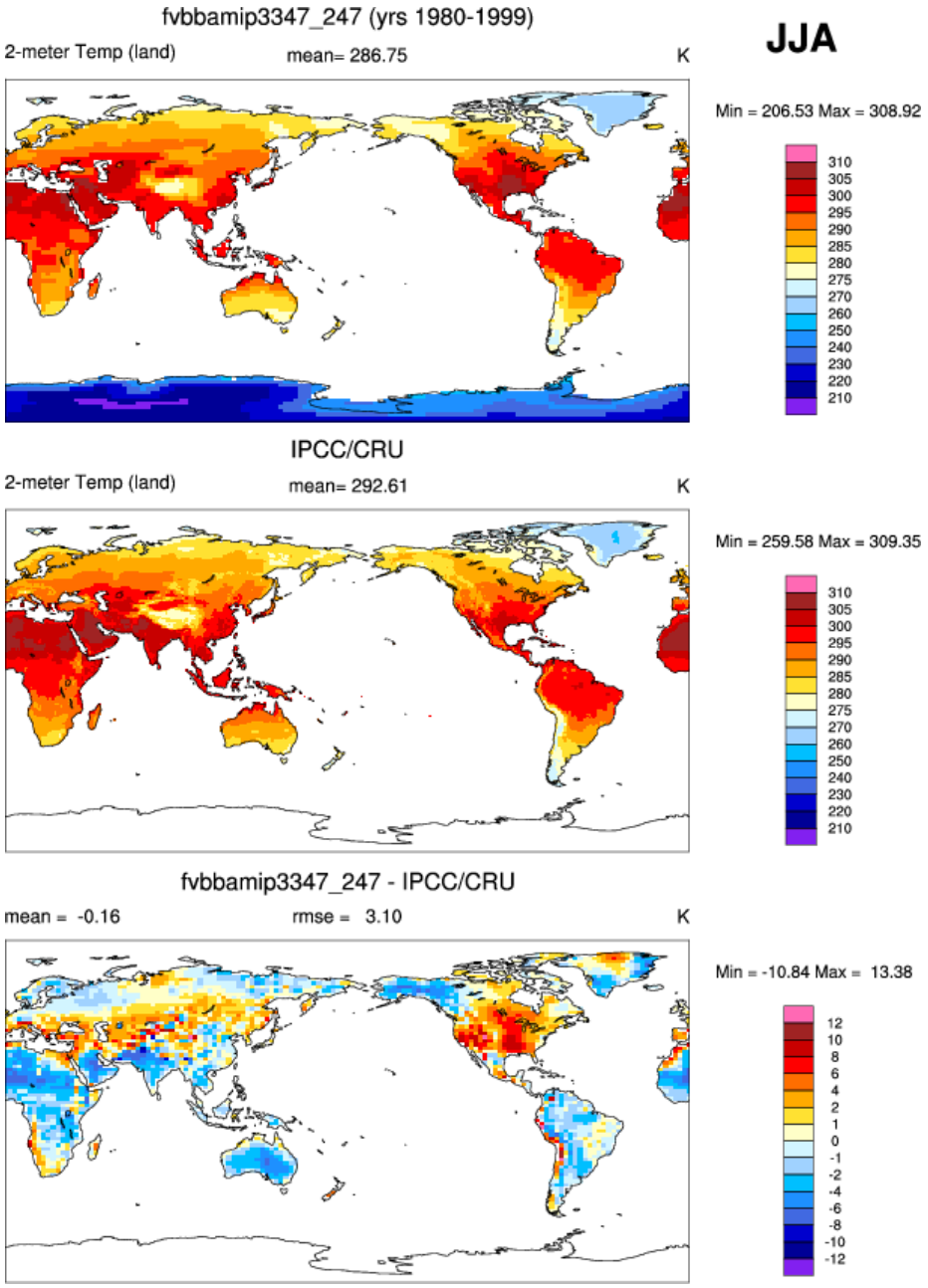

The error pattern in surface air temperature (figure 9, bottom panel) for resolution configuration *bb* persists in higher-resolution cases *cc* and *dd* (Figure 10). While the global-mean temperature bias remains roughly the same in configuration *cc* (-0.17 deg K, Figure 10, top panel) as in *bb* (-0.16 deg K, Figure 9, bottom panel), the simulation degrades further in configuration *dd* (-0.27 deg K, Figure 10, bottom panel). However, the global **rmse** remains roughly the same across all resolutions.

Figure 10: As in Figure 8, except for JJA-average model-observational differences in continental surface air temperature for CAM3.3 configurations *cc* (top panel) and *dd* (bottom panel).

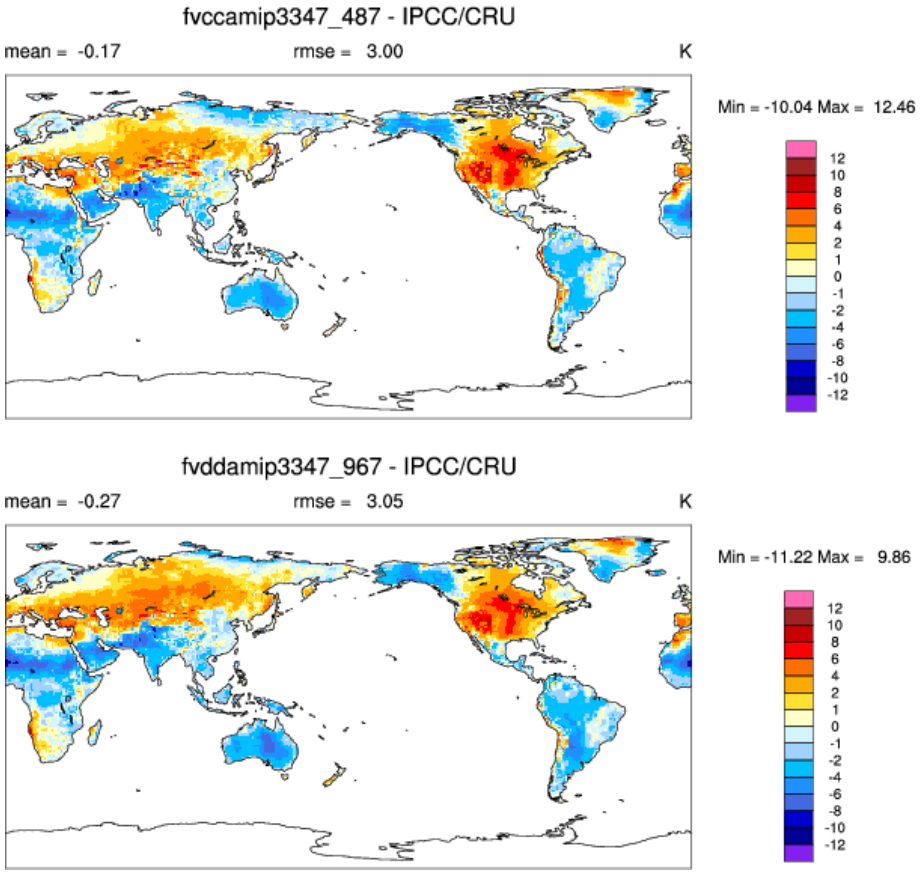

The JJA-average precipitation rate simulated in resolution configuration *bb* (Figure 11, top panel) differs substantially from that of observations (Figure 11, middle panel), as indicated by the comparable magnitudes of the global **rmse** (2.1 mm day^{-1}, bottom panel) and the observed global-mean precipitation rate (2.6 mm day^{-1}, middle panel).

Figure 11: As in Figure 7, except for the JJA-average CAM3.3 precipitation rate in resolution configuration *bb* (top panel, expressed in mm day^{-1}) compared with Global Precipitation Climatology Project (GPCP) observations (middle panel). JJA-average model-observational differences, as well as the associated global-mean bias and **rmse**, are shown in the bottom panel.

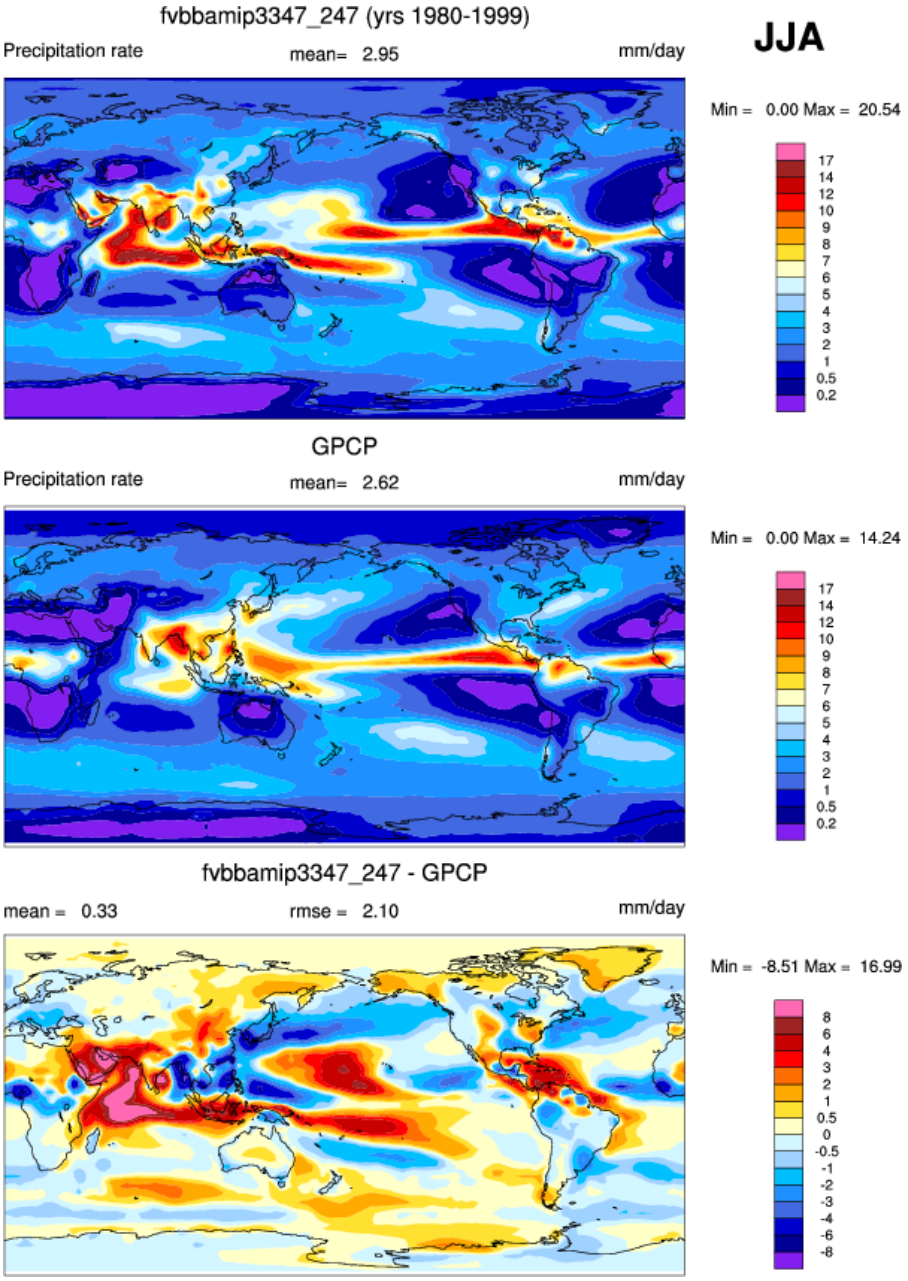

The mean seasonal precipitation differences are largest over tropical oceans. Here the rainfall amounts associated with the Intertropical Convergence Zone (ITCZ) are poorly simulated in many locations, and the model produces a spurious double ITCZ over the Indian and Tropical West Pacific Oceans as well. Model-observational precipitation differences also are relatively large over most continental areas, especially where monsoonal and/or orographic effects (e.g. Himalayan and U.S. Rocky Mountain regions) are important influences on JJA seasonal precipitation.

The error pattern displayed at the coarsest *bb* resolution (Figure 11, bottom panel) remains qualitatively the same at higher resolutions *cc* and *dd* (Figure 12). However, unlike other examined model variables, the global-mean bias and **rmse** of precipitation decrease incrementally with increasing horizontal resolution.

Figure 12: As in Figure 8, except for the JJA-average model-observational differences in precipitation rate for CAM3.3 resolution configurations *cc* (top panel) and *dd* (bottom panel).

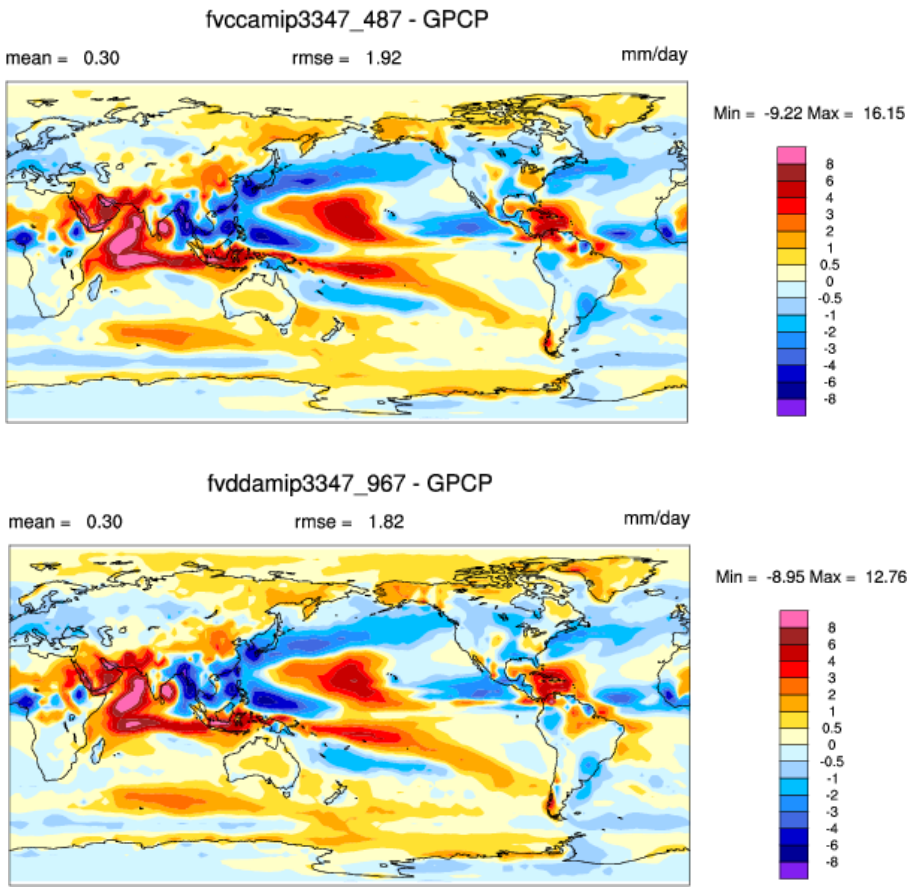

3.3 *Annual cycles of selected atmospheric climatic variables over irrigated regions*

As a way of evaluating the model's ability to correctly track the temporal variations of climate variables, it is also worthwhile to compare the annual cycle of simulated monthly means with corresponding observations. For our application, it is especially useful if the climate variables are spatially averaged over regions of the globe where irrigation is extensively practiced.

Once again, we evaluate the model total cloud cover, surface air temperature, and precipitation rate, but now on regional scales. In Figure 13, for example, the simulated annual cycles of these variables for horizontal-resolution configurations *bb*, *cc*, and *dd* are compared with the observations over a "Southwestern U.S." region that includes the Rocky Mountains and areas west and south below latitude 42 N.

Figure 13: Annual cycle of total (vertically integrated) cloud cover (expressed as a % area), surface air temperature (in deg K), and precipitation rate (in mm day^{-1}), all averaged over a Southwestern U.S. region. Model simulations for resolution configurations *bb (*1.89x2.50 degrees latitude-longitude), *cc* (0.94x1.25 degrees latitude-longitude), and *dd* (0.47x0.63 degrees latitude-longitude) are denoted by, respectively, brown, green, and blue dashed lines; the observations (datasets from SRB: Surface Radiation Budget, ERA15: ECMWF reanalysis, and GPCP: Global Precipitation Climatology Project) are denoted by solid black lines.

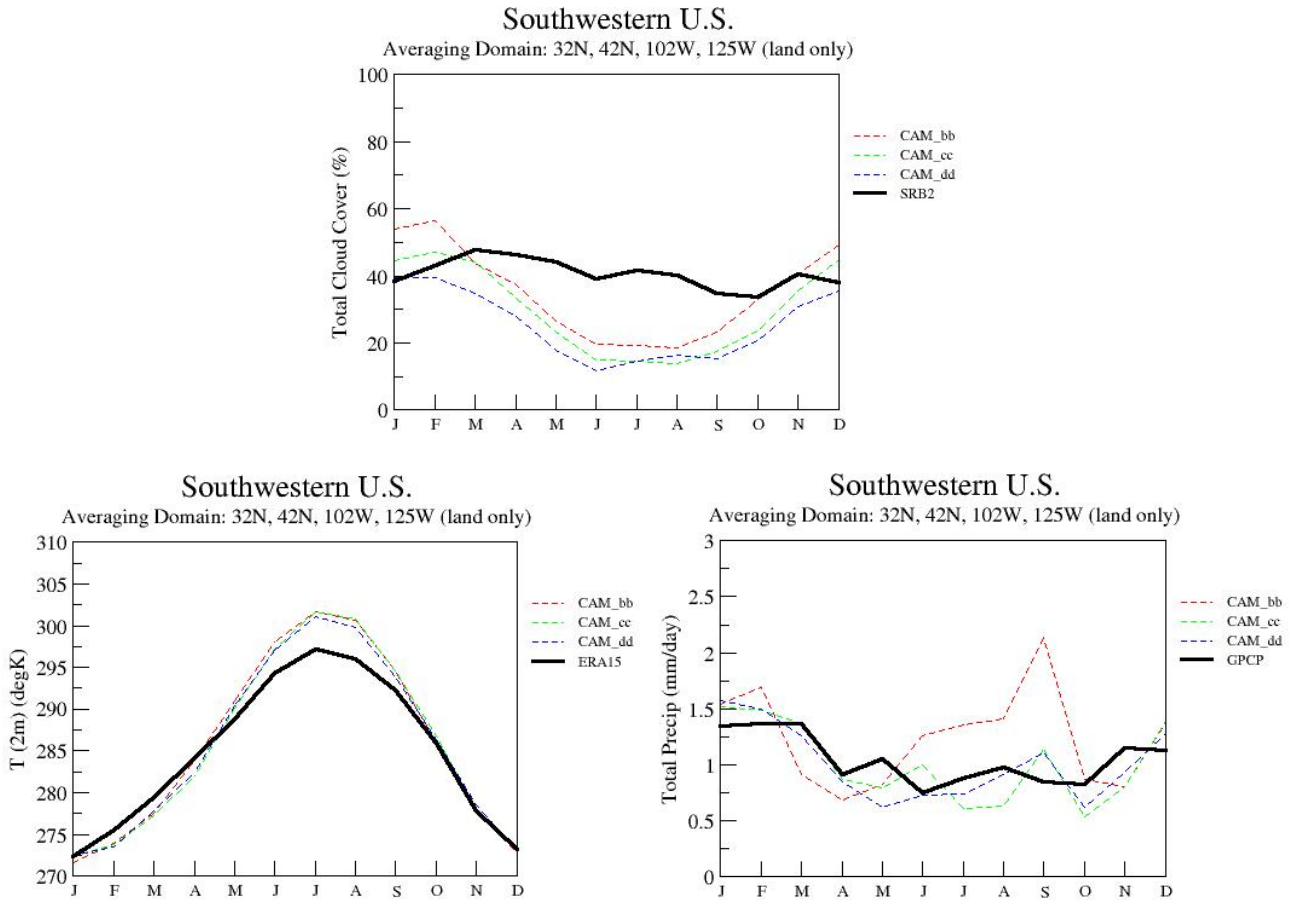

Except during the winter months, the model generally under-estimates cloud cover, but somewhat more so at the higher-resolutions configurations *cc* and *dd*. Consistent with this simulation deficiency, surface air temperature is biased positive during the warmer months of the year, and without much sensitivity to increasing resolution. The annual cycle of precipitation rate is fairly well-simulated at the two finer horizontal resolutions *cc* and *dd*; but for configuration *bb,* it is positively biased in summer.

This anomalous behavior is probably due to a less realistic simulation of orographic effects, which can only be coarsely represented at the *bb* resolution. Limiting the evaluation to just the California-Nevada sector (thereby removing the Rocky Mountain sub-region) eliminates the positive precipitation bias at resolution *bb* (Figure 14, bottom right panel). This result suggests that simulating precipitation in the vicinity of the Rockies is especially problematical at the coarsest resolution *bb*. (Note also that both the observed and modeled annual cycles of precipitation in the larger Southwestern U.S. region are quite different from those in the California-Nevada sector.)

Figure 14: As in Figure 13, except for spatial averaging over California and Nevada only.

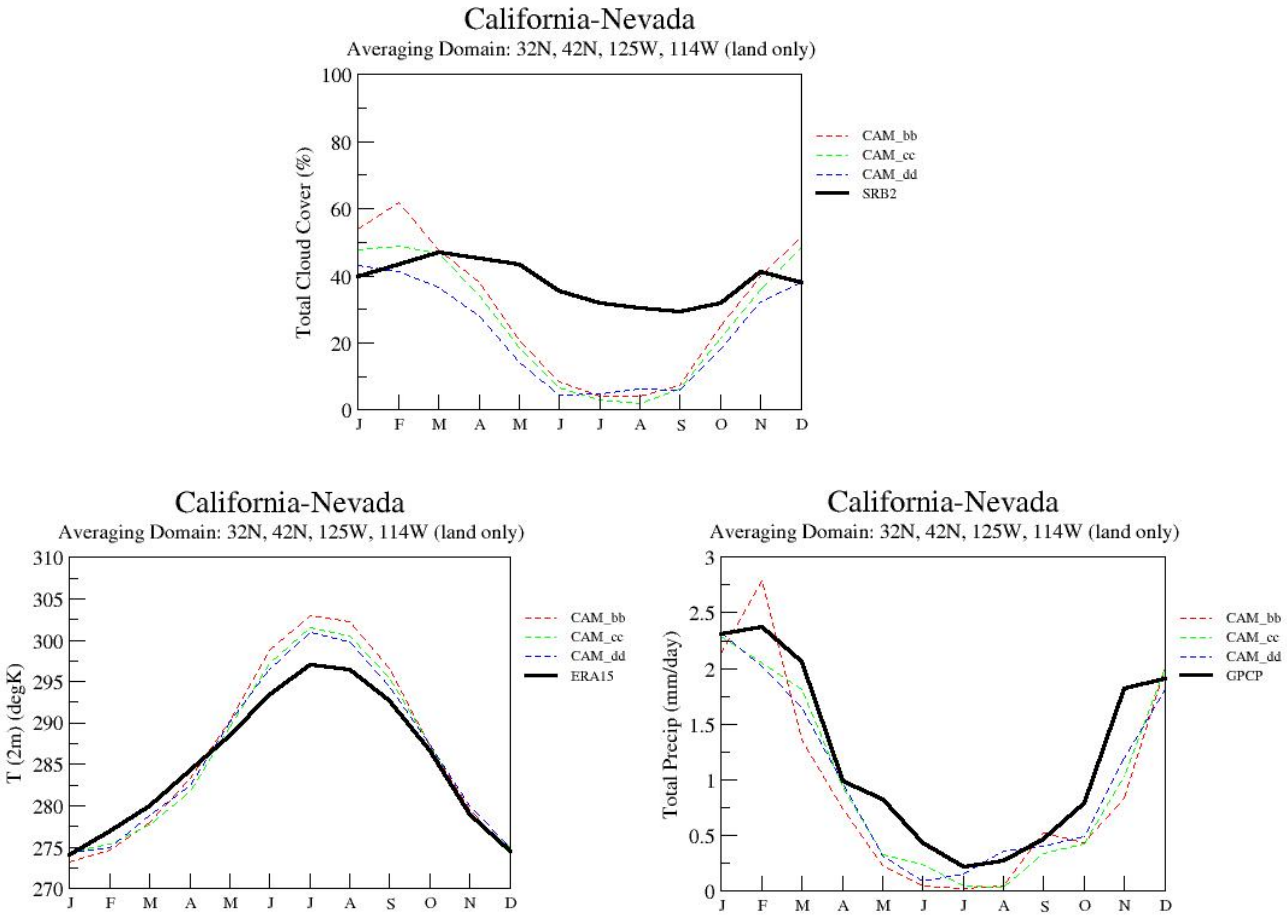

The annual cycles of the selected climate variables are qualitatively different over Northern India (Figure 15). The CAM3.3 cloud cover is too extensive at all resolutions, except during the winter and early spring. Model surface air temperature also is generally somewhat too warm in these same months when model cloud cover is too scant, but seems fairly insensitive to cloud-cover biases during the remainder of the year. The latter results are not wholly unexpected, since surface temperatures during the Indian summer and winter monsoons are strongly influenced by transverse ocean-continent heat transfers in addition to the local energy forcings. At all resolutions, CAM3.3 simulates overly abundant precipitation and also initiates Indian summer monsoon precipitation too early. Although the precipitation differences across resolution configurations are not very substantial, the model produces a marginally better simulation for the configurations *cc* and *dd* than for the coarsest *bb* resolution.

Figure 15: As in Figure 13, except for spatial averaging over Northern India.

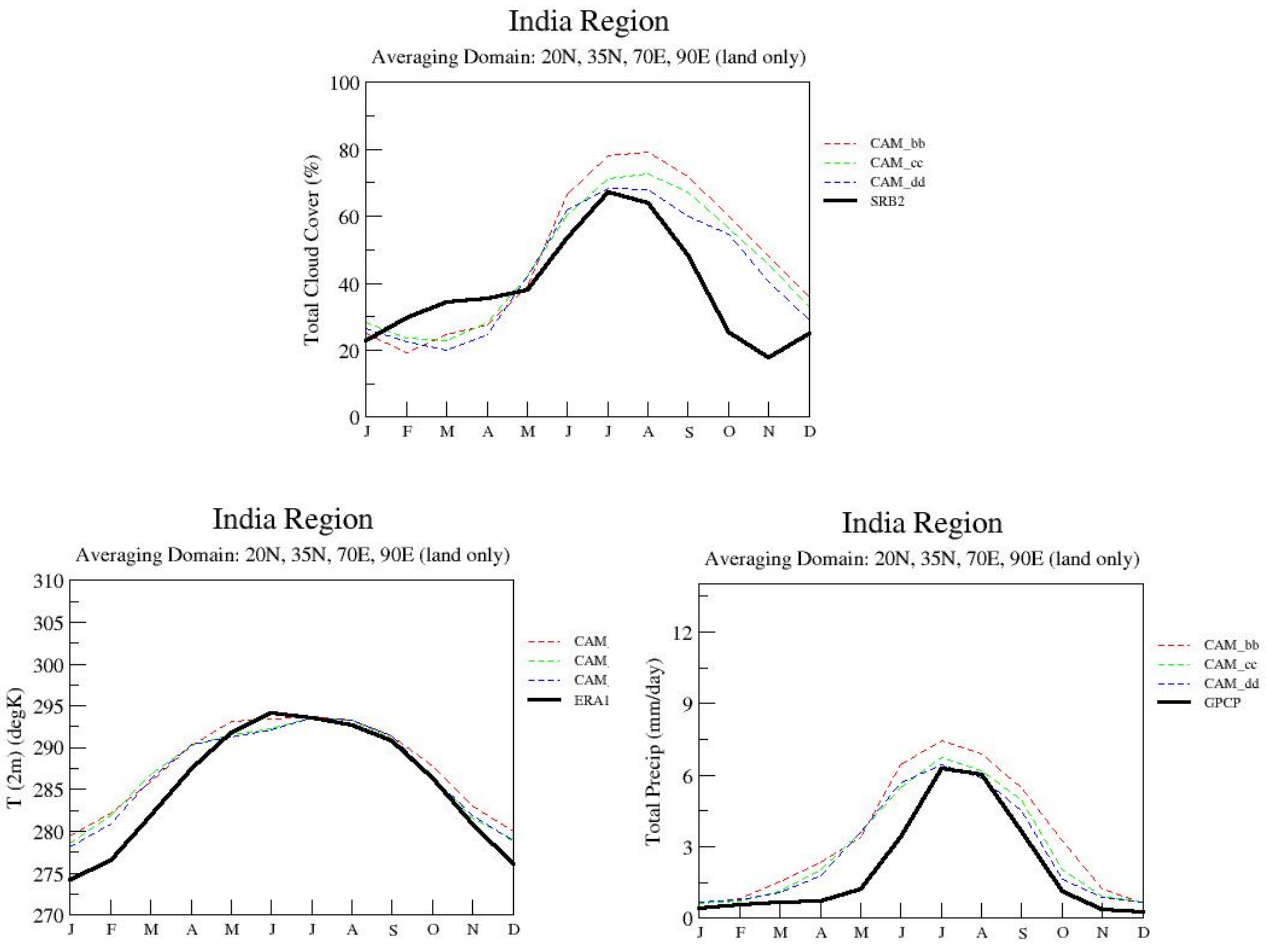

In contrast, over Northeast China the annual cycle of precipitation is especially well-simulated, while the positive biases found in model surface temperatures during much of the year are fairly consistent with a correspondingly under-estimated total cloud cover (Figure 16). Increasing horizontal resolution also produces little change in simulation performance.

Figure 16: As in Figure 13, except for spatial averaging over Northeast China

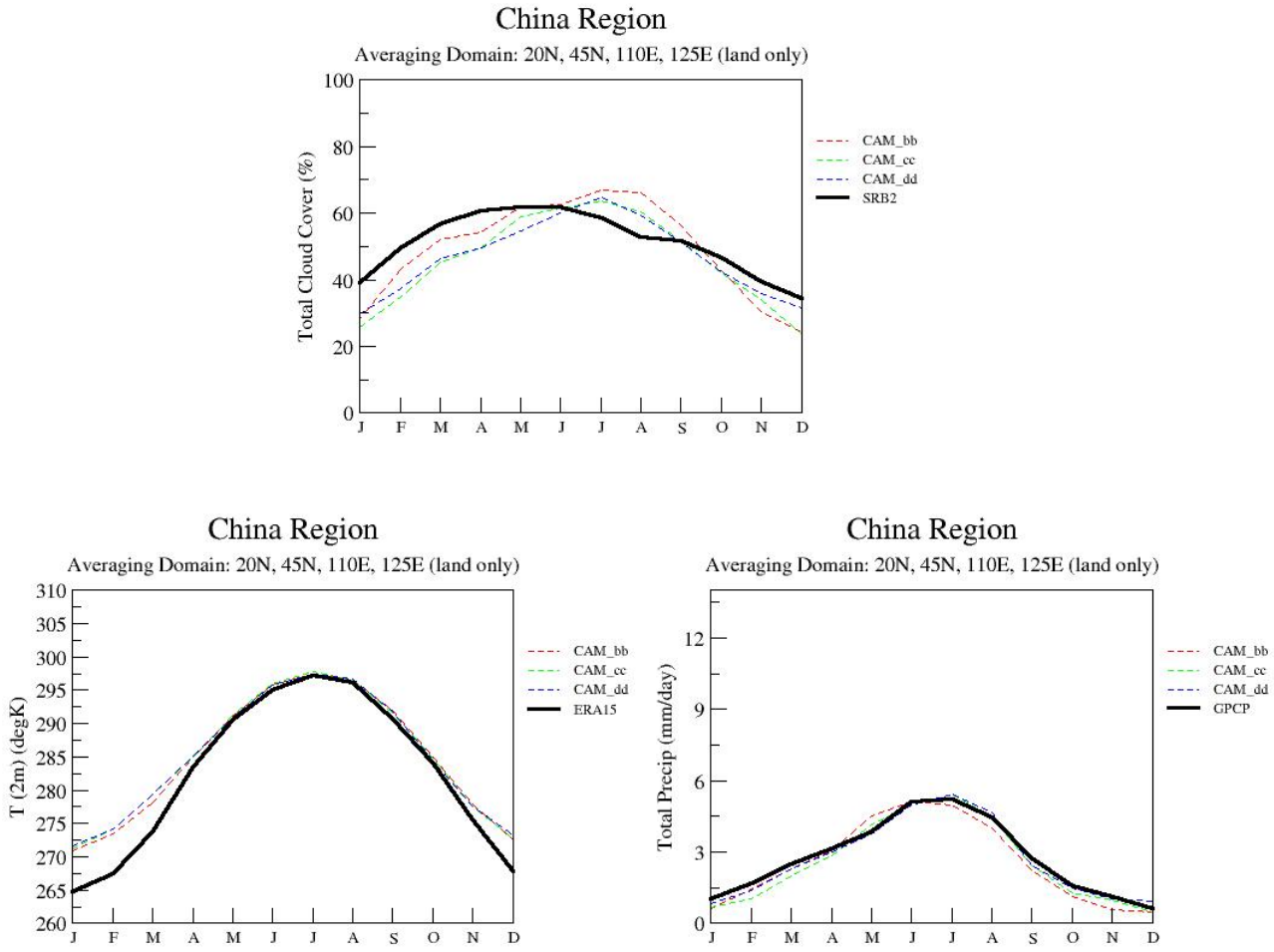

4. Summary

As the initial effort of an LDRD project on the climatic effects of agricultural irrigation practices, we have performed numerical control experiments with the CAM3.3 atmospheric climate model operated in a finite volume (FV) dynamical representation, and with prescribed standard AMIP ocean boundary conditions. We implemented the control experiments at three horizontal resolutions, with associated mesh sizes 1.89x2.50, 0.94x1.25, and 0.47x0.63 degrees latitude-longitude. The model's performance was generally acceptable, although a number of persistent errors in the climate simulations were apparent. It should be noted, however, that such shortcomings are typical of current-generation models.

The increases in horizontal resolution mostly did not ameliorate model biases evident at coarser resolutions. Hence, the extra computational costs required to run the climate model at finer horizontal resolutions do not produce commensurate payoffs in its overall performance. In fact, increases in model horizontal resolution tend to produce a somewhat degraded simulation of a number of climate variables, as indicated by statistical metrics such as global-mean bias and root-mean square error.

A possible reason for this phenomenon is that the model developers have "tuned" the parameterizations of subgrid-scale physical processes for a standard horizontal resolution (e.g. the 1.89x2.50-degrees latitude-longitude grid of configuration *bb*); thus, without further tuning on our part, the model performs somewhat more poorly at higher resolutions. However, the simulation of precipitation is an important exception to this general trend: its representation improves incrementally at higher resolutions, both in a global and regional sense, especially where orography plays an important role in determining the local hydroclimate.

Appendix: Technical Details of CAM3.3 Control Experiments

Here we describe further details of the features of the CAM3.3 (archive tag cam3_3_47) and of our control experiments performed with it.

A major innovation of the CAM3 model line is that a finite volume (FV) representation of atmospheric variables and forcings may be chosen, where the evolution of model variables is predicted in Lagrangian control volumes whose horizontal dimensions are defined by a specified latitude-longitude grid spacing. In the FV implementation of the CAM3.3, a two-dimensional conservative semi-Lagrangian tracer-advection scheme is used to represent transport within the control volumes, which themselves evolve in their vertical dimension. An attractive attribute of the FV representation is that the resulting simulations conserve global atmospheric mass and moisture to a high degree of numerical precision (see Lin and Rood 1997, Lin 2004, and Collins et al. 2004 for further details).

This FV implementation qualitatively differs from the Eulerian spectral (ES) representation, which was adopted in previous-generation CAM models, and which remains an option for the CAM3.3 model. In the ES representation, the spatial structure of the field variables is described by series of orthogonal global basis functions; hence, information from both upstream and downstream influences a particular point in space. In contrast, the FV representation maintains local calculation of spatial derivatives and allows mainly upstream influences to operate, assuring that the spatial relationships among different variables are maintained. The FV representation also prevents the occurrence of Gibbs oscillations (high wave-number distortions) that are especially prevalent in ES depictions of atmospheric climate in the vicinity of mountains.

In the ES version of the CAM3.3 model, the series of orthogonal basis functions is truncated at wave number 85 (denoted as "spectral T85" resolution). At this truncation, a spectral model is able to resolve phenomena at spatial scales roughly equivalent to that of a grid having 128 points in the latitudinal direction and 256 points in the longitudinal direction (Collins et al. 2006a). We ran the FV version of CAM3.3 at three different horizontal resolutions corresponding to latitude-longitude mesh sizes of 1.89x2.50 degrees (96 x 144 grid points), 0.94x1.25 degrees (192 x 288 grid points), and 0.47x0.63 degrees (384 x 576 grid points)--designated as resolution configurations *bb*, *cc*, and *dd*, respectively. Thus, the *cc* and *dd* resolution configurations of the FV version of the model were able to explicitly simulate phenomena at spatial scales finer than the ES spectral T85 CAM3.3.

The semi-Lagrangian FV representation also permits a longer time step than would otherwise be needed to maintain the numerical stability of a standard finite-difference representation of climate variables near the poles, where the longitudinal meridians (and hence the control volume boundaries) converge. The CAM3.3 physics time step was 30 minutes for all resolution configurations, while the tracer-advection time step was 30 minutes, 15 minutes, and 7.5 minutes for, respectively, resolution configurations *bb*, *cc*, and *dd*. For each of these configurations, the dynamics time step was specified to be one-fourth of the corresponding tracer-advection value.

We used the same sub-grid scale physical parameterizations as provided in the standard FV CAM3.3 code, except for some minor adjustments of selected parameters for the *dd* configuration. These parameter changes ensured a rough agreement of radiation fluxes and cloud/moisture characteristics with those of an ES T85 run, and also served to maintain a rough balance between net short-wave and long-wave fluxes (i.e. approximate radiative equilibrium) at the top of the model atmosphere. These parameter adjustments were as follows for resolution configuration *dd*:

- In the cloud liquid water scheme *cldwat.F90*, parameter *icritc,* the threshold ice mixing ratio that must be satisfied for auto-conversion of liquid water to snow in cold clouds to occur, was increased from 18.0×10^{-6} to 45.0×10^{-6}. This change was necessary in order to obtain a reasonable cloud ice-water content.

- In the cloud fraction scheme *cldwat.F90,* pressure parameter *premit* was reduced from a value of 75000 Pa (750 mb) to 25000 Pa (250 mb). The effect of this change was to specify that a relative-humidity threshold for the formation of middle clouds (at pressure level p between 750 mb and 250 mb) would be determined by linear interpolation of the relative humidity threshold values for low clouds (those below 750 mb) and for high clouds (those above 250 mb). (The former *premit* value of 25000 Pa effectively assigned identical relative-humidity thresholds for low and middle clouds.)

- In the shallow convection scheme *hk_conv.F90*, the precipitation efficiency parameter *c0*, was reduced from a value of 1.0×10^{-4} to 5.0×10^{-5} in order to maintain realistic amounts of convective precipitation production.

We ran CAM3.3 with Atmospheric Model Intercomparison Program (AMIP) monthly average sea surface temperatures (SSTs) and sea ice extents that were specified from observations and interpolated to the appropriate grid for each resolution configuration. We applied these ocean boundary conditions for the period from 1 September 1978 through 31 December 1999, where daily values were derived by interpolating linearly between the same days of neighboring months. Allowing for a model "spin-up" between 1 September 1978 and 31 December 1979, we compared these three AMIP control simulations of the climate of 1 January 1980 through 31 December 1999 with available observations for the same period.

All of the CAM3.3 experiments were run on massively parallel Linux *Peloton* clusters at the Open Computing Facility (OCF) of the Lawrence Livermore National Laboratory using the Intel ic91_new compiler. The *bb* and *cc* configurations typically used 168 and 336 processors, respectively, while the *dd* configuration used 512 or 768 processors, depending on the computational platform. Throughput ranged from 24 simulated years per computation day for the *bb* configuration on 168 processors to 3 simulated years per day for the *dd* configuration on 512 processors.

We stored model data output files on the PCMDI-managed server *Nonstop*. (Data from the irrigation sensitivity experiments at 1.94x2.50-degree and 0.47x0.63-degree resolutions also were stored on *Nonstop*. Future hardware changes may require moving these model data to another server.)

Diagnostic plots of several dozen model climatic variables and their differences from available observations also were generated using software developed by the NCAR Atmospheric Model Working Group (AMWG). These plots (some of which are displayed in this report) are currently accessible on the PCMDI website at the following URLs for the CAM3.3 *bb*, *cc*, and *dd* resolution configurations:

http://www-pcmdi.llnl.gov/Outgoing/cam3/bb/fvbbamip3347_247-obs/index.html

http://www-pcmdi.llnl.gov/Outgoing/cam3/cc/fvccamip3347_487-obs/index.html

http://www-pcmdi.llnl.gov/Outgoing/cam3/dd/fvddamip3347_967-obs/index.html

Acknowledgments

The work of LDRD Project 06-ERD-066 was performed under the auspices of the U.S. Department of Energy by Lawrence Livermore National Laboratory under Contract DE-AC52-07NA27344.

References

Collins, W.D., and Coauthors, 2004: Description of the NCAR Community Atmosphere Model (CAM3). Tech. Rep. NCAR/TN-464+STR, National Center for Atmospheric Research, Boulder, Colorado, 226 pp.

Collins, W.D., and Coauthors, 2006a: The formulation and atmospheric simulation of the Community Atmosphere Model Version 3 (CAM3). *Journal of Climate*, **19**, 2144-2161.

Collins, W.D., and Coauthors, 2006b: The Community Climate System Model version 3 (CCSM3), *Journal of Climate*, **19**, 2122-2143.

Gates, W. L., 1992: AMIP: The Atmospheric Model Intercomparison Project, *Bulletin of the American Meteorological Society,* **73**, 1962-1970.

Gates, W.L., J.S. Boyle, C. Covey, C.G. Dease, C.M. Doutriaux, R.S. Drach, M. Fiorino, P.J. Gleckler, J.J. Hnilo, S.M. Marlais, T.J. Phillips, G.L. Potter, B.D. Santer, K.R. Sperber, K.E. Taylor, and D.N. Williams, 1999: An overview of the results of the Atmospheric Model Intercomparison Project (AMIP *). Bulletin of the American Meteorological Society*, **80**, 29-55.

Lin, S.-J., 2004. A "vertically Lagrangian" finite-volume dynamical core for global models. *Monthly Weather Rev*iew, **132**, 2293-2307.

Lin, S-J., and R.B. Rood, 1996: Multidimensional flux-form semi-Lagrangian transport schemes. *Monthly Weather Rev*iew, **124**, 2046-2070.

Oleson, K.W., and Coauthors, 2004: Technical description of the Community Land Model (CLM). Tech. Rep. NCAR/TN-461+STR, National Center for Atmospheric Research, Boulder, Colorado, 174 pp.